

Spatio-Temporal Relation and Attention Learning for Facial Action Unit Detection

Zhiwen Shao¹, Lixin Zou², Jianfei Cai³, Yunsheng Wu⁴, Lizhuang Ma¹

¹ Shanghai Jiao Tong University ² Tsinghua University

³ Monash University ⁴ Tencent YouTu

shaozhiwen@sjtu.edu.cn, zoulx15@mails.tsinghua.edu.cn, jianfei.cai@monash.edu, simonwu@tencent.com, ma-lz@cs.sjtu.edu.cn

Abstract

Spatio-temporal relations among facial action units (AUs) convey significant information for AU detection yet have not been thoroughly exploited. The main reasons are the limited capability of current AU detection works in simultaneously learning spatial and temporal relations, and the lack of precise localization information for AU feature learning. To tackle these limitations, we propose a novel spatio-temporal relation and attention learning framework for AU detection. Specifically, we introduce a spatio-temporal graph convolutional network to capture both spatial and temporal relations from dynamic AUs, in which the AU relations are formulated as a spatio-temporal graph with adaptively learned instead of predefined edge weights. Moreover, the learning of spatio-temporal relations among AUs requires individual AU features. Considering the dynamism and shape irregularity of AUs, we propose an attention regularization method to adaptively learn regional attentions that capture highly relevant regions and suppress irrelevant regions so as to extract a complete feature for each AU. Extensive experiments show that our approach achieves substantial improvements over the state-of-the-art AU detection methods on BP4D and especially DISFA benchmarks.

1. Introduction

Facial action unit (AU) detection has recently attracted increasing attention in the communities of computer vision and affective computing [10, 21, 15, 9], as it plays a critical role in the applications of human-robot interaction and digital entertainment. Each facial AU is associated with one or more local muscle actions and captures fine-grained expression details, as defined in the Facial Action Coding System (FACS) [5]. AUs can spatially co-occur in certain expressions or can be mutually exclusive in any expression. Be-

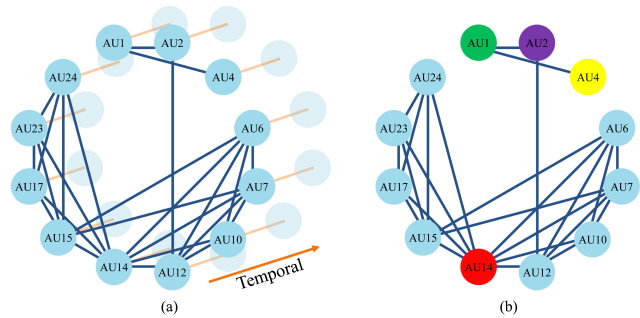


Figure 1. (a) An example of the spatio-temporal relation graph for 12 AUs. The spatial edges (dark blue) are defined based on statistical AU correlations in the training set, and the temporal edges (orange) connect the same AUs between consecutive frames. For easy illustration, we only show the spatial edges in the first frame. (b) The partition strategy of neighboring nodes, in which AU 14 is the gravity center (red). We partition the neighboring nodes into three classes: the root node (green), a centripetal node (purple) that has a equal or closer distance to the gravity center than the root node, and a centrifugal node (yellow) that is farther from the gravity center than the root node.

sides, each AU is dynamically changed across consecutive frames. However, most existing AU detection works have not thoroughly exploited the spatial and temporal relations among AUs, due to their limited capacities of relation learning and representation learning.

Earlier works [24, 11, 26, 25] employ probabilistic graphical models (PGMs) [17] including Bayesian network (BN), dynamic Bayesian network (DBN) and restricted Boltzmann machine (RBM) to model local pairwise AU dependencies or global AU dependencies. These methods resort to hand-crafted features, which limits the performance of AU relation reasoning. In addition, they only focus on local pairwise relations or implicit global relations, and ignore the spatio-temporal graph structure of AU relations.

Recently, by exploiting the prevailing deep learning technology, Corneanu *et al.* [4] proposed a deep struc-

ture inference network (DSIN) to infer the structure among AUs by iterative message passing, and Li *et al.* [9] used a gated graph neural network (GGNN) to capture correlations among AUs. However, the two methods crop predefined square regions to extract AU features based on prior knowledge, which ignores that AUs have irregular shapes and are non-rigidly changed across different facial expressions. Besides, they neglect the temporal AU dependencies. On the other hand, a few other methods [3, 6] utilize long short-term memory (LSTM) for temporal relation modeling without considering the spatial relations.

To tackle the above limitations, we propose a novel *Spatio-Temporal Relation and Attention Learning (STRAL)* framework for AU detection. In particular, instead of considering only spatial or temporal correlations, we introduce a spatio-temporal graph convolutional network [27] to simultaneously model spatial and temporal dependencies among AUs. As illustrated in Figure 1(a), a spatio-temporal relation graph is constructed based on statistical correlations and temporal dynamics of AUs. Since some pairs of the AUs connected by spatial edges have strong correlations and other pairs have weak correlations, our framework adaptively learns the weights of spatial edges for each spatio-temporal graph convolutional layer.

Moreover, we aim to learn AU representations without loss of useful information or bringing irrelevant information. Instead of cropping predefined regions, we propose an attention regularization method to adaptively learn regional attentions capturing the highly related regions so as to extract a complete feature for each AU. The regularization over attentions encourages preserving high responses in highly relevant regions and suppressing the responses in irrelevant regions. In our framework, the learned AU representations contribute to the further AU relation reasoning by the spatio-temporal graph convolutional network.

The main contributions of this paper are threefold: (i) We propose a novel spatio-temporal relation and attention learning framework for AU detection. To our knowledge, this is the first work of introducing the spatio-temporal graph convolutional network for AU detection. (ii) We propose an attention regularization method, which can capture highly relevant regions and suppress irrelevant regions so as to extract complete AU features. (iii) Extensive experiments show that our approach soundly outperforms the state-of-the-art AU detection methods on BP4D and more significantly on DISFA.

2. Related Work

We review the previous techniques that are closely relevant to our work, including relation learning based AU detection and region learning based AU detection.

Relation Learning Based AU Detection. Considering the inherent correlations among AUs, many works perform AU

detection by exploiting the AU relations. Due to the capability of modeling complex data distributions, PGMs [17] have been extensively used for AU detection. Tong *et al.* [24] utilized a BN to model the local pairwise dependencies such as co-occurrence and mutual exclusion among AUs. Li *et al.* [11] employed a DBN for joint facial AU detection, expression recognition and landmark tracking, in which the local AU dependencies and local relations between AUs and landmarks are both reasoned. Wang *et al.* [26] proposed an interval temporal Bayesian network to capture complex spatio-temporal relations, in which the facial expression is treated as a complex activity containing overlapping or sequential primitive facial events. Instead of only modeling pairwise relations, Wang *et al.* [25] applied a RBM to capture both local AU dependencies and implicit global AU correlations. All these methods are based on hand-crafted features and overlook the spatio-temporal graph structure of AU relations, which limits their performance of learning AU relations.

Recently, there are some AU detection works combining relation learning with the prevailing deep learning technology. Chu *et al.* [3] and He *et al.* [6] used deep convolutional networks to extract the facial feature of each frame and then used LSTMs to model the temporal correlations within consecutive frames. Corneanu *et al.* [4] proposed the DSIN to capture AU relations by explicitly passing information between AU predictions. Li *et al.* [9] built an AU relation graph and introduced a GGNN to learn the spatial correlations among AUs. However, these methods do not simultaneously model spatial and temporal relations.

Region Learning Based AU Detection. Current AU detection methods often crop square regions or apply regional attentions to extract AU representations. Since facial landmarks can predefine rough locations of AUs based on prior knowledge, Zhao *et al.* [29] selected regions centered at certain landmarks to extract scale-invariant feature transform (SIFT) [13] features for each AU. Instead of selecting predefined regions, Zhao *et al.* [30] uniformly partitioned a feature map into local regions, and applied independent convolutional filters to process each local region. Corneanu *et al.* [4] utilized an independent convolutional network to extract a feature from each predefined image patch, while Li *et al.* [9] first used a convolutional network over the input image to extract a global feature map and then process each cropped feature from the global feature map. These methods treat each position in the cropped region with the same importance, which may lose significant information.

Inspired by the great success of attention mechanism in the computer vision field [8, 1, 18], a few works exploit the attentions of AUs to extract relevant features. Li *et al.* [10] utilized predefined locations of AU centers to generate a square region with a fixed size and a fixed attention distribution for AUs, in which a position with a farther Man-

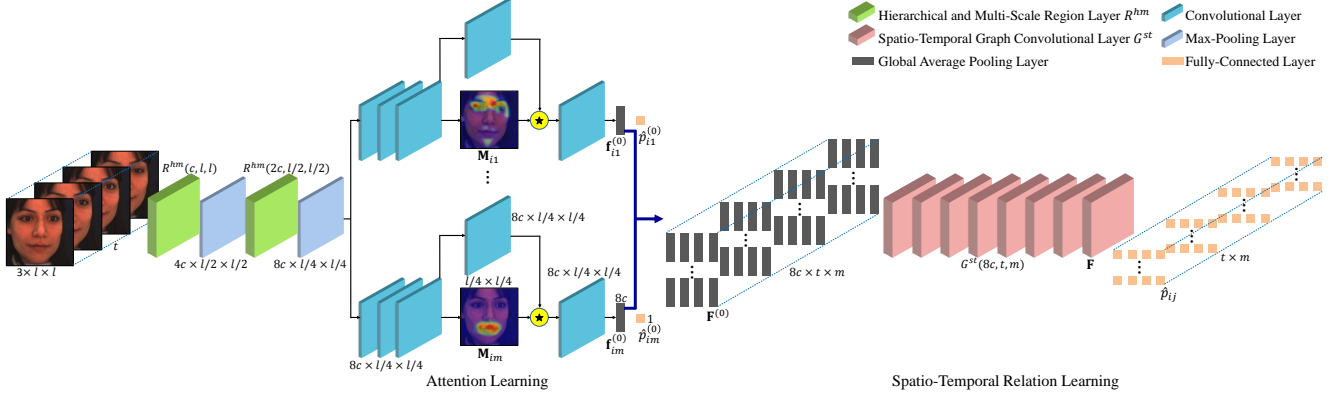


Figure 2. The architecture of our STRAL framework. Given a sequence of t frames, our framework first extracts features of m AUs for each frame by the attention learning, and further uses the spatio-temporal relation learning to simultaneously predict AU occurrence probabilities of all the t frames. The learned attention map is overlaid on the input first frame for better viewing, in which the shown examples M_{i1} and M_{im} correspond to AUs 4 and 25 respectively. “ \star ” denotes element-wise multiplication of the attention map and each feature map channel. The expression $c' \times l' \times l'$ denotes that the channel, height and width of the corresponding layer are c' , l' and l' , respectively.

hattan distance to the AU center has a lower attention. Due to the availability of AU intensities, Sanchez *et al.* [19] employed the AU intensity to determine the amplitude and size of a Gaussian distribution so as to generate an attention map for each AU. These methods cannot adapt to different AUs with irregular shapes and non-rigid transformations. Shao *et al.* [21] adopted an adaptive attention learning module to refine the predefined spatial attention of each AU, and Shao *et al.* [22] further directly learned spatial and channel-wise attentions of AUs without the prior knowledge. The refined attentions learned in [21] are only highlighted in the neighboring regions of the predefined attentions, and the attentions learned in [22] also capture some irrelevant regions. In contrast, we propose an attention regularization method to capture the highly related regions while suppressing irrelevant regions.

3. STRAL for Facial AU Detection

3.1. Overview

Given consecutive t frames with the same size of $3 \times l \times l$, our main goal is to predict their AU occurrence probabilities $\{\hat{p}_1, \dots, \hat{p}_t\}$, where $\hat{p}_i = (\hat{p}_{i1}, \dots, \hat{p}_{im})$, and m is the number of AUs. Figure 2 illustrates the architecture of our framework. We first utilize a deep convolutional network with a similar structure to ARL [22] to extract features of m AUs for each frame. Specifically, the input frame first goes through two hierarchical and multi-scale region layers [21], each of which is followed by a max-pooling layer. The detailed structure of a hierarchical and multi-scale region layer R^{hm} is shown in Figure 3(a). It contains an input layer and three hierarchical intermediate layers with different scales of partitioned patches, in which each patch is processed with independent convolutional kernels to extract

local features. The multi-scale features learned by the hierarchical and multi-scale region layers are further processed by m branches, each of which employs the attention regularization to learn regional attentions so as to extract a relevant feature for an AU. Then, we utilize a spatio-temporal graph convolutional network [27] to process the combined AU features of all the t frames by learning spatial and temporal AU correlations, and simultaneously predict their AU occurrence probabilities.

3.2. Attention Learning

As shown in Figure 2, we adopt a one-channel convolutional layer followed by a sigmoid function to learn an attention map M_{ij} with size $l/4 \times l/4$ for the j -th AU of the i -th frame, where $i = 1, \dots, t$, and $j = 1, \dots, m$. To capture highly related information for the j -th AU, we element-wise multiply M_{ij} with each channel of an intermediate feature map to regionally weight the feature map. The learned AU feature $f_{ij}^{(0)}$ with a size of $8c$ is obtained by further applying a convolutional layer and a global average pooling layer [12].

To supervise the learning of each AU feature $f_{ij}^{(0)}$, we use the last one-dimensional fully-connected layer followed by a sigmoid function to obtain the initially estimated AU occurrence probability $\hat{p}_{ij}^{(0)}$. Then, we employ an AU detection loss for $\hat{p}_{ij}^{(0)}$, which is defined as

$$\mathcal{L}^u = - \frac{1}{t} \sum_{i=1}^t \sum_{j=1}^m w_j [p_{ij} \log \hat{p}_{ij}^{(0)} + (1 - p_{ij}) \log (1 - \hat{p}_{ij}^{(0)})], \quad (1)$$

where p_{ij} denotes the ground-truth occurrence probability of the j -th AU in the i -th frame, and w_j is a weight param-

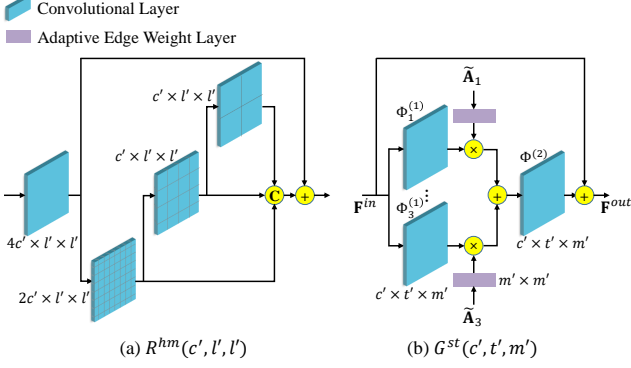


Figure 3. The structures of a hierarchical and multi-scale region layer $R^{hm}(c', l', l')$ and a spatio-temporal graph convolutional layer $G^{st}(c', t', m')$. “C” denotes concatenation of feature map channels.

ter [21] to weight the loss of the j -th AU for alleviating the data imbalance issue. We set $w_j = (1/o_j) / \sum_{k=1}^m (1/o_k)$, in which o_j is the occurrence rate of the j -th AU in the training set.

Although \mathcal{L}^u can encourage M_{ij} to capture all the relevant regions, some irrelevant regions may also have certain responses, which negatively impacts the performance of AU detection. To only preserve the attentions in highly relevant regions, we propose an attention regularization term to constrain the learned attention maps:

$$\mathcal{R}(M_{ij}) = \frac{1}{l/4 \times l/4} \sum_{a=1}^{l/4} \sum_{b=1}^{l/4} M_{ijab}, \quad (2)$$

where $M_{ijab} \in (0, 1)$ denotes the attention weight in the a -th row and the b -th column of M_{ij} . The attention regularization essentially uses the L1 norm to ensure the sparsity of attention weights so as to suppress insignificant attentions. By combining Eqs. (1) and (2), we obtain the full loss in the attention learning stage:

$$\mathcal{L}^a = \mathcal{L}^u + \lambda^r \frac{1}{mt} \sum_{i=1}^t \sum_{j=1}^m \mathcal{R}(M_{ij}), \quad (3)$$

where λ^r is a hyper-parameter to weigh the importance of the attention regularization. In this stage, all the convolutional layers employ 3×3 kernels with stride (1, 1) and padding (1, 1), and all the max-pooling layers process 2×2 spatial fields with stride (2, 2).

3.3. Spatio-Temporal Relation Learning

To model the correlations among intra- and inter-frame AUs simultaneously, we combine the features $\mathbf{f}_{ij}^{(0)}$ of m AUs in all the t frames, in which the combined feature $\mathbf{F}^{(0)}$ with size $8c \times t \times m$ is further input to a spatio-temporal

graph convolutional network. As illustrated in Figure 2, there are eight $G^{st}(8c, t, m)$ layers in the graph convolutional network. The elaborated structure of $G^{st}(c', t', m')$ is shown in Figure 3(b), in which the convolution operations are based on the spatio-temporal graph structure of AU relations.

Spatio-Temporal Graph Construction. We construct an undirected spatio-temporal AU relation graph $G = (V, E)$, where the node set $V = \{v_{ij} | i = 1, \dots, t, j = 1, \dots, m\}$ contains all the m AUs in the t frames, and the edge set E consists of a spatial edge subset E^s and a temporal edge subset E^t . To determine spatial edges, we compute the Pearson’s correlation coefficient (PCC) between each pair of the j -th and k -th AUs in the training set, denoted as r_{jk} . Then, we can define $E^s = \{v_{ij}v_{ik} | r_{jk} \geq \tau, i = 1, \dots, t, j = 1, \dots, m, k = j + 1, \dots, m\}$, where τ is a threshold to divide positive and non-positive relations, and a spatial edge is included if the corresponding AU pair has a positive relation. E^t includes edges between the same AUs in consecutive frames, which is defined as $E^t = \{v_{ij}v_{(i+1)j} | i = 1, \dots, t - 1, j = 1, \dots, m\}$. In this way, we obtain $E = E^s \cup E^t$. An example of the spatio-temporal AU relation graph G is illustrated in Figure 1(a).

After defining G , we can obtain its adjacency matrix \mathbf{A} with a size of $m \times m$ in a single frame, in which A_{jk} and A_{kj} are both 1 if $v_{1j}v_{1k} \in E^s$ and are both 0 otherwise, and $A_{jj} = 1$ as self-connections, $j = 1, \dots, m, k = j + 1, \dots, m$. To achieve the graph convolution, we normalize \mathbf{A} as:

$$\tilde{\mathbf{A}} = \mathbf{A}\mathbf{\Lambda}, \quad (4)$$

where $\mathbf{\Lambda}$ is a diagonal matrix. Each diagonal element of $\mathbf{\Lambda}$ is defined as

$$\Lambda_{jj} = \begin{cases} (\sum_{k=1}^m A_{jk})^{-1} & \text{if } \sum_{k=1}^m A_{jk} > 0, \\ 0 & \text{if } \sum_{k=1}^m A_{jk} = 0. \end{cases} \quad (5)$$

Graph Convolution for AU Relation Learning. Considering AUs are spatially located in facial regions and there are different spatial characteristics in AU correlations, we cluster different spatial correlations following [27]. As illustrated in Figure 1(b), the neighboring nodes are partitioned into three classes: the root node itself, a centripetal node that has a equal or closer distance to the gravity center than the root node, and a centrifugal node that is farther from the gravity center than the root node. The gravity center is defined as the AU with the most neighboring nodes. Specifically, we dismantle $\tilde{\mathbf{A}}$ into three matrices $\{\tilde{\mathbf{A}}_1, \tilde{\mathbf{A}}_2, \tilde{\mathbf{A}}_3\}$ with $\tilde{\mathbf{A}} = \sum_{q=1}^3 \tilde{\mathbf{A}}_q$:

$$\begin{cases} \tilde{A}_{1jj} = \tilde{A}_{jj} & j = 1, \dots, m, \\ \tilde{A}_{2jk} = \tilde{A}_{jk} & \text{if } d_k \leq d_j, j = 1, \dots, m, k \neq j, \\ \tilde{A}_{3jk} = \tilde{A}_{jk} & \text{if } d_k > d_j, j = 1, \dots, m, k \neq j, \end{cases} \quad (6)$$

where the elements of $\tilde{\mathbf{A}}_q$ are 0 otherwise, and d_j is the hop distance between the j -th AU and the gravity center in the graph G .

Note that in Figure 1(a), several AU pairs have close relations like usually co-occurred AU 1 (inner brows raise) and AU 2 (outer brows raise), and several AU pairs have weak relations such as AU 7 (eyelids tighten) and AU 12 (lip corners pull) which do not necessarily co-occur. This motivates us to utilize adaptively learned instead of fixed weights for spatial edges. As shown in Figure 3(b), for a spatio-temporal graph convolutional layer $G^{st}(8c, t, m)$, we input $\tilde{\mathbf{A}}_q$ to an adaptive edge weight layer, in which a learnable weight matrix with size $m \times m$ followed by a tanh function is element-wise multiplied with $\tilde{\mathbf{A}}_q$ to obtain a new matrix $\dot{\mathbf{A}}_q$.

In this way, we formulate the spatio-temporal relation learning process in G^{st} as

$$\mathbf{F}^{out} = \Phi^{(2)}\left(\sum_{q=1}^3 \dot{\mathbf{A}}_q \Phi_q^{(1)}(\mathbf{F}^{in})\right) + \mathbf{F}^{in}, \quad (7)$$

where \mathbf{F}^{in} and \mathbf{F}^{out} are the input and output features respectively, and $\Phi_q^{(1)}(\cdot)$ and $\Phi^{(2)}(\cdot)$ denote the convolution operations in the parallel convolutional layers and the last convolutional layer, respectively. The three parallel convolutional layers using 1×1 convolutional kernels with stride $(1, 1)$ and padding $(0, 0)$ capture spatial correlations, and the last convolutional layer using $t^k \times 1$ convolutional kernels with stride $(1, 1)$ and padding $((t^k - 1)/2, 0)$ captures temporal correlations, where t^k is the temporal kernel size. The residual structure [7] is adopted to avoid the vanishing gradient problem.

Spatio-Temporal Relation Learning for AU Detection.

As illustrated in Figure 2, with eight spatio-temporal graph convolutional layers, our STRAL framework can model spatio-temporal correlations among all the m AUs in the t frames. We partition the output feature \mathbf{F} of the last spatio-temporal graph convolutional layer into a new feature \mathbf{f}_{ij} with the size of $8c$ for each AU, which is beneficial for final AU detection due to the integration of correlated information from other AUs and frames, $i = 1, \dots, t$, $j = 1, \dots, m$. Similar to the attention learning stage, we adopt a one-dimensional fully-connected layer followed by a sigmoid function to obtain the finally estimated AU occurrence probability \hat{p}_{ij} , respectively. The AU detection loss \mathcal{L}^u in Eq. (1) is further applied to \hat{p}_{ij} to enable the training of the spatio-temporal graph convolutional network.

4. Experiments

4.1. Datasets and Settings

Datasets. We evaluate our framework on two benchmark datasets BP4D [28] and DISFA [14], each of which is an-

notated by certified FACS experts.

BP4D consists of 41 subjects with 23 females and 18 males, in which each subject participates in 8 sessions. There are totally 328 videos including about 140,000 frames with AU occurrence labels. Similar to previous works [30, 10, 21], we conduct subject-exclusive 3-fold cross-validation on 12 AUs: 1, 2, 4, 6, 7, 10, 12, 14, 15, 17, 23 and 24, in which two folds are used for training and the rest one is used for testing.

DISFA contains 12 female and 15 male subjects, each of whom is recorded by a video with 4,845 frames. Each frame is annotated with AU intensities on a six-point ordinal scale from 0 to 5. It exhibits a more serious data imbalance issue than BP4D, in which most AUs have very low occurrence rates. Following the settings of previous works [30, 10, 21], we treat an AU as occurrence if its intensity is equal or greater than 2 and treat it as non-occurrence otherwise. We also conduct a subject-exclusive 3-fold cross-validation on 8 AUs: 1, 2, 4, 6, 9, 12, 25 and 26.

Implementation Details. Our framework is implemented based on PyTorch [16]. As with the previous techniques [21, 22], each image is aligned to $3 \times 200 \times 200$ using similarity transformation, and is further randomly cropped to $3 \times l \times l$ and mirrored. The crop size l , the structure hyper-parameter c , the number of frames t in an input sequence, and the temporal kernel size t^k are set to 176, 8, 48, and 5, respectively. The number of AUs m is 12 for BP4D and 8 for DISFA, the threshold τ is 0.15, and the hyper-parameter λ^r is 10^{-4} . We employ the SGD solver, a mini-batch size of 8, a Nesterov momentum of 0.9, and a weight decay of 0.0005. We first train the attention learning stage for up to 12 epochs with initial learning rate of 0.006, and then train the spatio-temporal relation learning stage for up to 24 epochs with initial learning rate of 0.02. The learning rate is multiplied by a factor of 0.3 at every 2 and 6 epochs for attention learning and spatio-temporal relation learning, respectively.

Following the setting of ARL [22], the attention learning network trained on DISFA is initialized with the parameters of the well-trained model for BP4D, in which the branches of AUs 9, 25 and 26 unavailable in BP4D are initialized from correlated AUs 10, 23 and 24 respectively. In each experiment of the 3-fold cross-validation, we construct the spatio-temporal AU relation graph G based on the PCC results in the training set with 2 folds. At test time, our framework can predict the AU occurrence probabilities of an input sequence with any number of frames, which has flexible applicability.

Evaluation Metrics. We report two commonly used metrics for AU detection: frame-based F1-score (F1-frame) and accuracy. F1-frame is formulated as $F1 = 2PR/(P + R)$, where P and R denote precision and recall, respectively.

AU	F1-Frame									Accuracy				
	DRML	EAC	DSIN	JAA	CMS	LP	SRERL	ARL	STRAL	EAC	JAA	CMS	ARL	STRAL
1	36.4	39.0	51.7	47.2	49.1	43.4	46.9	45.8	48.2	68.9	74.7	55.9	73.9	77.6
2	41.8	35.2	40.4	44.0	44.1	38.0	45.3	39.8	47.7	73.9	80.8	67.7	76.7	78.1
4	43.0	48.6	56.0	54.9	50.3	54.2	55.6	55.1	58.1	78.1	80.4	71.5	80.9	82.4
6	55.0	76.1	76.1	77.5	79.2	77.1	77.1	75.7	75.8	78.5	78.9	81.3	78.2	77.6
7	67.0	72.9	73.5	74.6	74.7	76.7	78.4	77.2	78.1	69.0	71.0	71.9	74.4	76.4
10	66.3	81.9	79.9	84.0	80.9	83.8	83.5	82.3	81.6	77.6	80.2	77.3	79.1	78.2
12	65.8	86.2	85.4	86.9	88.3	87.2	87.6	86.6	87.6	84.6	85.4	87.4	85.5	85.8
14	54.1	58.8	62.7	61.9	63.9	63.3	60.6	58.8	60.5	60.6	64.8	57.4	62.8	63.6
15	33.2	37.5	37.3	43.6	44.4	45.3	52.2	47.6	50.2	78.1	83.1	71.6	84.7	84.3
17	48.0	59.1	62.9	60.3	60.3	60.5	63.9	62.1	64.0	70.6	73.5	73.7	74.1	71.6
23	31.7	35.9	38.8	42.7	41.4	48.1	47.1	47.4	51.2	81.0	82.3	74.6	82.9	82.3
24	30.0	35.8	41.6	41.9	51.2	54.2	53.3	55.4	55.2	82.4	85.4	84.1	85.7	82.5
Avg	48.3	55.9	58.9	60.0	60.6	61.0	62.9	61.1	63.2	75.2	78.4	72.9	78.2	78.4

Table 1. F1-frame and accuracy results for 12 AUs on BP4D. The reported results of previous methods are from their papers. EAC-Net, JAA-Net and LP-Net are shortly written as EAC, JAA and LP, respectively.

AU	F1-Frame									Accuracy				
	DRML	EAC	DSIN	JAA	CMS	LP	SRERL	ARL	STRAL	EAC	JAA	CMS	ARL	STRAL
1	17.3	41.5	42.4	43.7	40.2	29.9	45.7	43.9	52.2	85.6	93.4	91.6	92.1	94.9
2	17.7	26.4	39.0	46.2	44.3	24.7	47.8	42.1	47.4	84.9	96.1	94.7	92.7	93.5
4	37.4	66.4	68.4	56.0	53.2	72.7	59.6	63.6	68.9	79.1	86.9	79.9	88.5	89.5
6	29.0	50.7	28.6	41.4	57.1	46.8	47.1	41.8	47.8	69.1	91.4	82.6	91.6	90.4
9	10.7	80.5	46.8	44.7	50.3	49.6	45.6	40.0	56.7	88.1	95.8	95.2	95.9	96.8
12	37.7	89.3	70.8	69.6	73.5	72.9	73.5	76.2	72.5	90.0	91.2	87.8	93.9	92.4
25	38.5	88.9	90.4	88.3	81.1	93.8	84.3	95.2	91.3	80.5	93.4	86.3	97.3	94.9
26	20.1	15.6	42.2	58.4	59.7	65.0	43.6	66.8	67.6	64.8	93.2	80.7	94.3	94.0
Avg	26.7	48.5	53.6	56.0	57.4	56.9	55.9	58.7	63.0	80.6	92.7	87.3	93.3	93.3

Table 2. F1-frame and accuracy results for 8 AUs on DISFA. The results of different AUs for most previous methods fluctuate significantly due to the severe data imbalance problem.

The average results of F1-frame and accuracy over all AUs (abbreviated as Avg) are also shown. In the following sections, all the F1-frame and accuracy results are reported in percentage with “%” omitted.

4.2. Comparison with State-of-the-Art Methods

We compare our method against state-of-the-art AU detection methods under the same subject-exclusive 3-fold cross-validation setting. These methods include DRML [30], EAC-Net [10], DSIN [4], JAA-Net [21], CMS [20], LP-Net [15], SRERL [9] and ARL [22]. Note that most of these approaches use outside training data or additional facial landmark labels, while our method only uses the benchmark dataset with only AU labels. Specifically, EAC-Net and SRERL fine-tune the official pre-trained VGG19 [23] model, CMS utilizes outside thermal images to guide the representation learning, and LP-Net pre-trains its network on a face recognition dataset VG-Face2 [2] and then fine-tunes on the benchmark dataset. Besides, DSIN and SRERL crop AU regions centered at

certain landmarks, EAC-Net and JAA-Net predefine AU attentions based on landmark locations, and LP-Net employs facial shape regularization formed by landmarks to facilitate AU detection.

Evaluation on BP4D. Table 1 shows the F1-frame and accuracy results of our method STRAL and state-of-the-art methods on BP4D benchmark. We can see that our STRAL outperforms all the previous methods in terms of either F1-frame or accuracy metric, in which the average F1-frame is advanced from level 62 to level 63. Compared to the methods like LP-Net and SRERL that use additional training images and landmark labels, our STRAL achieves better performance with only benchmark training images and AU labels, which demonstrates our framework has a strong capability of suppressing the model overfitting. Note that our STRAL performs better than the state-of-the-art SRERL which also exploits the graph structure of AU relations. The gain comes from the effective AU features learned by our proposed attention regularization.

Evaluation on DISFA. We report the F1-frame and accu-

AU	F1-Frame					Accuracy				
	AL	AL+ \mathcal{R}	AL+ \mathcal{R} + G^{sf}	AL+ \mathcal{R} + G^{sa}	STRAL	AL	AL+ \mathcal{R}	AL+ \mathcal{R} + G^{sf}	AL+ \mathcal{R} + G^{sa}	STRAL
1	47.9	47.6	48.4	48.5	48.2	77.9	79.3	78.5	76.9	77.6
2	38.7	41.4	44.6	46.6	47.7	79.4	79.1	80.2	77.7	78.1
4	49.3	57.0	51.7	55.0	58.1	78.0	81.7	80.9	84.1	82.4
6	74.0	75.6	75.6	76.7	75.8	76.9	77.8	77.8	78.3	77.6
7	75.7	77.8	77.6	77.8	78.1	74.3	75.2	76.1	76.1	76.4
10	80.8	81.0	81.9	81.8	81.6	77.8	77.7	78.1	78.6	78.2
12	87.3	86.9	86.7	87.0	87.6	85.9	85.5	85.5	85.5	85.8
14	57.1	61.3	61.2	61.5	60.5	61.6	63.1	63.9	63.6	63.6
15	49.7	47.3	47.6	50.5	50.2	83.6	84.0	83.9	83.7	84.3
17	63.2	62.2	63.0	63.8	64.0	73.6	69.5	71.8	73.3	71.6
23	48.3	47.9	48.9	49.1	51.2	82.3	83.5	82.6	81.9	82.3
24	50.4	51.1	51.8	53.0	55.2	84.0	82.1	81.8	82.3	82.5
Avg	60.2	61.4	61.6	62.6	63.2	77.9	78.2	78.4	78.5	78.4

Table 3. F1-frame and accuracy results for 12 AUs of different variants of our STRAL on BP4D. AL: attention leaning without the attention regularization; \mathcal{R} : attention regularization; G^{sf} : graph convolutional network with only the spatial edge subset E^s and fixed all-ones edge weight matrices; G^{sa} : graph convolutional network with only the spatial edge subset E^s and adaptive edge weight layers. STRAL: our full model built on top of AL+ \mathcal{R} + G^{sa} by further considering the temporal correlations in the graph convolutional network.

AU	F1-Frame					Accuracy				
	AL	AL+ \mathcal{R}	AL+ \mathcal{R} + G^{sf}	AL+ \mathcal{R} + G^{sa}	STRAL	AL	AL+ \mathcal{R}	AL+ \mathcal{R} + G^{sf}	AL+ \mathcal{R} + G^{sa}	STRAL
1	52.1	54.1	53.2	53.5	52.2	94.8	94.5	94.3	94.3	94.9
2	30.9	40.2	49.6	47.0	47.4	89.4	92.8	95.0	94.7	93.5
4	71.5	69.1	71.9	69.7	68.9	91.0	89.8	90.4	89.5	89.5
6	44.0	44.5	43.2	48.5	47.8	91.3	91.1	92.0	90.4	90.4
9	44.8	50.5	47.6	55.1	56.7	95.4	95.5	96.1	96.8	96.8
12	73.0	72.3	70.7	74.6	72.5	93.7	93.0	92.4	93.5	92.4
25	93.5	92.2	89.9	91.7	91.3	96.3	95.5	93.8	95.2	94.9
26	53.7	64.8	58.5	57.1	67.6	91.7	92.8	88.1	89.9	94.0
Avg	58.0	61.0	60.6	62.2	63.0	93.0	93.1	92.8	93.0	93.3

Table 4. F1-frame and accuracy results for 8 AUs of different variants of our STRAL on DISFA.

racy results on DISFA in Table 2. It can be observed that our STRAL significantly outperforms all the previous approaches with large margins, due to the effectiveness of our proposed spatio-temporal relation learning. In particular, STRAL outperforms the state-of-the-art ARL by 4.3 in terms of average F1-frame, substantially improving the performance on DISFA. Moreover, there is a more serious data imbalance issue in DISFA than BP4D, which results in large performance fluctuations over different AUs for most of the previous approaches, especially EAC-Net, DSIN and LP-Net. In contrast, our STRAL achieves more stable performance across different AUs.

By comparing Table 1 and Table 2, we can see that SRERL achieves a good performance of average F1-frame 62.9 on BP4D while only 55.9 on DISFA, which suggests that SRERL has a limited generalization ability and thus restricts its applicability. In contrast, our STRAL obtains consistently top performance on BP4D and DISFA with average F1-frame of 63.2 and 63.0, respectively. Although JAA-

Net and ARL achieve similar accuracy results as ours, their F1-frame results are significantly lower on both BP4D and DISFA. This is because achieving a high F1-frame is more challenging than achieving a high accuracy, which is due to the data imbalance issue. Specifically, for those AUs with very low occurrence rates, directly predicting them as non-occurrences can obtain high accuracy but poor F1-frame results.

4.3. Ablation Study

In this section, we evaluate the effectiveness of each component in our STRAL framework. Tables 3 and 4 present the F1-frame and accuracy results of different variants of our framework on BP4D and DISFA benchmarks, respectively. AL is a baseline method which only contains the attention learning network without the attention regularization by setting $\lambda^r = 0$.

Effectiveness of Attention Regularization. After applying the attention regularization, AL+ \mathcal{R} improves the aver-

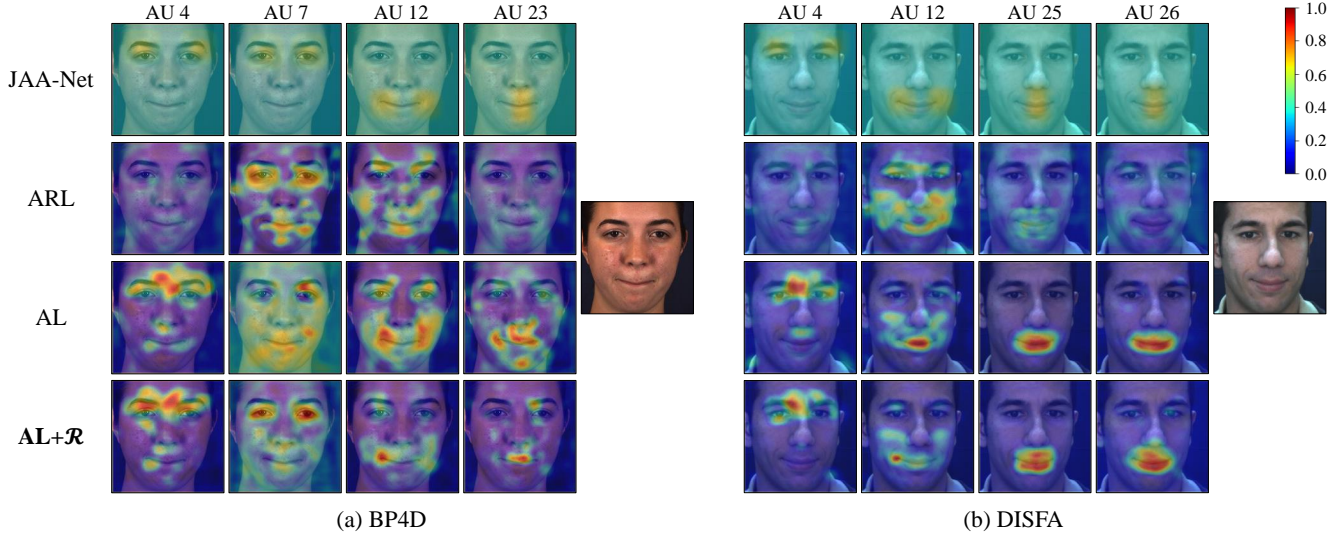


Figure 4. Visualization of the learned attention maps for several AUs of an example BP4D image and an example DISFA image. Each row shows the results of the same method. Attention weights are visualized using the colors shown in the color bar, which are overlaid on images.

age F1-frame from 60.2 and 58.0 to 61.4 and 61.0 over AL on BP4D and DISFA, respectively. We can see that AL+ \mathcal{R} has already outperformed the state-of-the-art ARL on BP4D and more significantly on DISFA, which indicates the effectiveness of our proposed attention regularization.

In addition, we visualize the learned attention maps of JAA-Net, ARL, AL and AL+ \mathcal{R} for two example images in Figure 4. We can observe that the learned attention maps of JAA-Net are only highlighted in the neighboring regions of predefined AU centers, which ignores useful information in other highly correlated regions. AL and ARL have rich responses in the whole face including some regions with less correlation, in which the captured irrelevant information may negatively influence the performance. In contrast, AL+ \mathcal{R} can suppress responses in irrelevant regions by employing the attention regularization. Besides, we can see AL+ \mathcal{R} obtains similar attention maps as AL for AUs 25 and 26 of the DISFA image, which indicates AL+ \mathcal{R} can preserve high responses in highly relevant regions. Our proposed attention regularization is beneficial for capturing all the highly related regions while suppressing irrelevant regions so as to extract complete AU features for AU detection.

Effectiveness of Spatio-Temporal Relation Learning.

Our proposed spatio-temporal relation learning models both spatial relations and temporal relations. We first investigate the effectiveness of spatial relation learning by only using the spatial edge subset E^s and setting the temporal kernel size $t^k = 1$. In Tables 3 and 4, we can observe AL+ \mathcal{R} + G^{sf} which element-wise multiplies fixed all-ones edge weight matrices with \mathbf{A}_q improves the results slightly on BP4D and performs worse on DISFA over AL+ \mathcal{R} . This is because

the strengths of correlations between different AU pairs are different, which should not be treated with the equal importance. In contrast, by adaptively learning edge weights, AL+ \mathcal{R} + G^{sa} improves the average F1-frame from 61.4 and 61.0 to 62.6 and 62.2 over AL+ \mathcal{R} on BP4D and DISFA, respectively.

After further learning the correlations among frames in a sequence, our STRAL achieves the best results on both BP4D and DISFA benchmarks. The spatial correlations and temporal correlations are simultaneously modeled by our spatio-temporal graph convolutional network, in which spatial and temporal relevant information are jointly exploited to improve the performance of AU detection. In our framework, the attention regularization contributes to extracting complete AU representations, and the spatio-temporal relation learning reasons spatial and temporal correlations based on the AU representations to improve the final performance.

5. Conclusion

In this paper, we have proposed a novel spatio-temporal relation and attention learning framework for AU detection. We have introduced a spatio-temporal graph convolutional network to capture both spatial and temporal correlations from dynamic AUs in consecutive frames. Moreover, we have proposed an attention regularization method to capture highly relevant regions and suppress irrelevant regions so as to extract complete AU representations. Extensive experiments have demonstrated that our approach soundly outperforms the state-of-the-art AU detection methods on BP4D and especially DISFA benchmarks. The achieved substantial improvement will contribute to the applications of AU

detection in human-robot interaction and digital entertainment fields.

References

- [1] Chunshui Cao, Xianming Liu, Yi Yang, Yinan Yu, Jiang Wang, Zilei Wang, Yongzhen Huang, Liang Wang, Chang Huang, Wei Xu, Deva Ramanan, and Thomas S Huang. Look and think twice: Capturing top-down visual attention with feedback convolutional neural networks. In *IEEE International Conference on Computer Vision*, pages 2956–2964. IEEE, 2015. 2
- [2] Qiong Cao, Li Shen, Weidi Xie, Omkar M Parkhi, and Andrew Zisserman. Vggface2: A dataset for recognising faces across pose and age. In *IEEE International Conference on Automatic Face and Gesture Recognition*, pages 67–74. IEEE, 2018. 6
- [3] Wen-Sheng Chu, Fernando De la Torre, and Jeffrey F Cohn. Learning spatial and temporal cues for multi-label facial action unit detection. In *IEEE International Conference on Automatic Face and Gesture Recognition*, pages 25–32. IEEE, 2017. 2
- [4] Ciprian A Corneanu, Meysam Madadi, and Sergio Escalera. Deep structure inference network for facial action unit recognition. In *European Conference on Computer Vision*, pages 309–324. Springer, 2018. 1, 2, 6
- [5] Paul Ekman and Erika L Rosenberg. *What the face reveals: Basic and applied studies of spontaneous expression using the Facial Action Coding System (FACS)*. Oxford University Press, USA, 1997. 1
- [6] Jun He, Dongliang Li, Bin Yang, Siming Cao, Bo Sun, and Lejun Yu. Multi view facial action unit detection based on cnn and blstm-rnn. In *IEEE International Conference on Automatic Face and Gesture Recognition*, pages 848–853. IEEE, 2017. 2
- [7] Kaiying He, Xiangyu Zhang, Shaoqing Ren, and Jian Sun. Deep residual learning for image recognition. In *IEEE Conference on Computer Vision and Pattern Recognition*, pages 770–778. IEEE, 2016. 5
- [8] Jason Kuen, Zhenhua Wang, and Gang Wang. Recurrent attentional networks for saliency detection. In *IEEE Conference on Computer Vision and Pattern Recognition*, pages 3668–3677. IEEE, 2016. 2
- [9] Guanbin Li, Xin Zhu, Yirui Zeng, Qing Wang, and Liang Lin. Semantic relationships guided representation learning for facial action unit recognition. In *AAAI Conference on Artificial Intelligence*, pages 8594–8601, 2019. 1, 2, 6
- [10] Wei Li, Farnaz Abtahi, Zhigang Zhu, and Lijun Yin. Eacnet: Deep nets with enhancing and cropping for facial action unit detection. *IEEE Transactions on Pattern Analysis and Machine Intelligence*, 40(11):2583–2596, 2018. 1, 2, 5, 6
- [11] Yongqiang Li, Shangfei Wang, Yongping Zhao, and Qiang Ji. Simultaneous facial feature tracking and facial expression recognition. *IEEE Transactions on Image Processing*, 22(7):2559–2573, 2013. 1, 2
- [12] Min Lin, Qiang Chen, and Shuicheng Yan. Network in network. In *International Conference on Learning Representations*, 2014. 3
- [13] David G Lowe. Object recognition from local scale-invariant features. In *IEEE International Conference on Computer Vision*, pages 1150–1157. IEEE, 1999. 2
- [14] S Mohammad Mavadati, Mohammad H Mahoor, Kevin Bartlett, Philip Trinh, and Jeffrey F Cohn. Disfa: A spontaneous facial action intensity database. *IEEE Transactions on Affective Computing*, 4(2):151–160, 2013. 5
- [15] Xuesong Niu, Hu Han, Songfan Yang, Yan Huang, and Shiguang Shan. Local relationship learning with person-specific shape regularization for facial action unit detection. In *IEEE Conference on Computer Vision and Pattern Recognition*, pages 11917–11926, 2019. 1, 6
- [16] Adam Paszke, Sam Gross, Soumith Chintala, Gregory Chanan, Edward Yang, Zachary DeVito, Zeming Lin, Alban Desmaison, Luca Antiga, and Adam Lerer. Automatic differentiation in pytorch. In *Advances in Neural Information Processing Systems Workshops*, 2017. 5
- [17] Judea Pearl. *Probabilistic reasoning in intelligent systems: Networks of plausible inference*. Morgan Kaufmann, 1988. 1, 2
- [18] Marco Pedersoli, Thomas Lucas, Cordelia Schmid, and Jakob J Verbeek. Areas of attention for image captioning. In *IEEE International Conference on Computer Vision*, pages 1242–1250. IEEE, 2017. 2
- [19] Enrique Sanchez, Georgios Tzimiropoulos, and Michel Valstar. Joint action unit localisation and intensity estimation through heatmap regression. In *British Machine Vision Conference*, page 233. BMVA Press, 2018. 3
- [20] Nishant Sankaran, Deen Dayal Mohan, Srirangaraj Setlur, Venugopal Govindaraju, and Dennis Fedorishin. Representation learning through cross-modality supervision. In *IEEE International Conference on Automatic Face and Gesture Recognition*, pages 1–8. IEEE, 2019. 6
- [21] Zhiwen Shao, Zhilei Liu, Jianfei Cai, and Lizhuang Ma. Deep adaptive attention for joint facial action unit detection and face alignment. In *European Conference on Computer Vision*, pages 725–740. Springer, 2018. 1, 3, 4, 5, 6
- [22] Zhiwen Shao, Zhilei Liu, Jianfei Cai, Yunsheng Wu, and Lizhuang Ma. Facial action unit detection using attention and relation learning. *IEEE Transactions on Affective Computing*, 2019. 3, 5, 6
- [23] Karen Simonyan and Andrew Zisserman. Very deep convolutional networks for large-scale image recognition. In *International Conference on Learning Representations*, 2015. 6
- [24] Yan Tong and Qiang Ji. Learning bayesian networks with qualitative constraints. In *IEEE Conference on Computer Vision and Pattern Recognition*, pages 1–8. IEEE, 2008. 1, 2
- [25] Ziheng Wang, Yongqiang Li, Shangfei Wang, and Qiang Ji. Capturing global semantic relationships for facial action unit recognition. In *IEEE International Conference on Computer Vision*, pages 3304–3311. IEEE, 2013. 1, 2
- [26] Ziheng Wang, Shangfei Wang, and Qiang Ji. Capturing complex spatio-temporal relations among facial muscles for facial expression recognition. In *IEEE Conference on Computer Vision and Pattern Recognition*, pages 3422–3429. IEEE, 2013. 1, 2

- [27] Sijie Yan, Yuanjun Xiong, and Dahua Lin. Spatial temporal graph convolutional networks for skeleton-based action recognition. In *AAAI Conference on Artificial Intelligence*, 2018. [2](#), [3](#), [4](#)
- [28] Xing Zhang, Lijun Yin, Jeffrey F Cohn, Shaun Canavan, Michael Reale, Andy Horowitz, Peng Liu, and Jeffrey M Girard. Bp4d-spontaneous: A high-resolution spontaneous 3d dynamic facial expression database. *Image and Vision Computing*, 32(10):692–706, 2014. [5](#)
- [29] Kaili Zhao, Wen-Sheng Chu, Fernando De la Torre, Jeffrey F Cohn, and Honggang Zhang. Joint patch and multi-label learning for facial action unit and holistic expression recognition. *IEEE Transactions on Image Processing*, 25(8):3931–3946, 2016. [2](#)
- [30] Kaili Zhao, Wen-Sheng Chu, and Honggang Zhang. Deep region and multi-label learning for facial action unit detection. In *IEEE Conference on Computer Vision and Pattern Recognition*, pages 3391–3399. IEEE, 2016. [2](#), [5](#), [6](#)